

See discussions, stats, and author profiles for this publication at: <https://www.researchgate.net/publication/258749905>

Thermally-Induced Dewetting in Ultra-Thin C₆₀ films on Copper Phthalocyanine

ARTICLE *in* THE JOURNAL OF PHYSICAL CHEMISTRY C · MARCH 2013

Impact Factor: 4.77 · DOI: 10.1021/jp4067372

CITATION

1

READS

53

3 AUTHORS, INCLUDING:



[Harald Werner Ade](#)

North Carolina State University

356 PUBLICATIONS 8,673 CITATIONS

[SEE PROFILE](#)

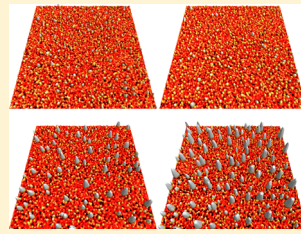
Thermally Induced Dewetting in Ultrathin C_{60} Films on Copper Phthalocyanine

T. McAfee, E. Gann, H. Ade, and D. B. Dougherty*

Department of Physics, North Carolina State University, Raleigh, North Carolina 27695, United States

 Supporting Information

ABSTRACT: The evolution of thermally annealed ultrathin fullerene– C_{60} layers on copper phthalocyanine is examined by atomic force microscopy and near-edge X-ray absorption fine structure spectroscopy. Annealing causes C_{60} films to dewet the copper phthalocyanine substrate surface via lateral surface mass transport. Coarsening of C_{60} clusters is observed that creates mounds that exceed the nominal C_{60} thickness by more than an order of magnitude and is consistent with surface diffusion-mediated mass transport. Implications for thermal morphology control in organic solar cells, such as the destabilization of multilayered C_{60} :CuPc with individual layers only ~5–10 nm thick, are discussed.



I. INTRODUCTION

Bilayer photovoltaic cells employing interfaces between copper phthalocyanine (CuPc) and fullerene– C_{60} were among the first to demonstrate that organic materials can provide a cost-effective alternative to the traditional inorganic solar cells.^{1,2} These materials are of interest due to their synthetic reproducibility in structure and the precise film thickness control offered by organic molecular beam deposition (OMBD) compared to solution-processed devices. While solution-processed polymer devices have recently defined the state-of-the-art in organic photovoltaic device performance with power conversion efficiencies reaching >8%,³ small-molecule devices, such as the CuPc: C_{60} bilayer, offer advantages in terms of precise composition control during vacuum evaporation and relative ease of integration into tandem architectures.⁴ CuPc: C_{60} bilayer films have also become important experimental and theoretical model systems in order to investigate the impact of molecular orientation at the heterojunction interface.^{5,6}

Recently, evaporated small-molecule organic photovoltaic (OPV) devices achieved a power conversion efficiency (PCE) of $6.6 \pm 0.2\%$ using a novel “donor–acceptor–acceptor” molecular architecture which increases both the short-circuit current (J_{sc}) and open-circuit voltage (V_{oc}) by manipulating the optical bandgap of the active material.⁷ However, such advances in control over the bandgaps of OPV materials may not be sufficient to reach the PCE needed to be cost-effective. A deeper understanding and control of the domain size, domain purity, and molecular orientation are crucial for achieving efficient exciton dissociation, charge transport, long-term device stability, and ultimately the PCE. Control of the film morphology in these devices is thus vital, and methodologies such as postdeposition thermal annealing need to be assessed for their efficacy as a control parameter.

The need for morphology control and manipulation has been recognized in efforts to grow mixed films of small molecules by vacuum codeposition in order to create intermixed morphol-

ogies analogous to those achieved in solution-processed bulk heterojunction (BHJ) solar cells.^{8,9} The BHJ morphology comprises a bicontinuous network of nanoscale donor and acceptor domains that is thought to be ideal for simultaneous optimization of exciton dissociation and free-carrier transport. Unfortunately, it is not always straightforward to achieve BHJ-like device performance using small-molecule codeposition. Morphologies and donor–acceptor connectivity can be degraded,⁹ and exciton dissociation efficiencies can be reduced.¹⁰ However, there have been notable successes¹¹ including a tandem cell with a high PCE of more than 6%.

Small-molecule intermixing strategies have been elaborated using the uniquely precise capabilities of OMBD growth to create compositionally graded solar cells by codeposition of C_{60} with CuPc and with boron sub-phthalocyanine.⁸ Holmes and co-workers showed that by creating films with controlled gradients in donor–acceptor composition, they could achieve improvements in PCE compared to simply codepositing the two materials to create a film with fixed composition. This clearly shows that it is possible to adjust OMBD growth conditions to improve the donor–acceptor networks in the OPV. More generally, controllable nanostructuring of donor–acceptor mixtures shows promise for solving the morphology problem for many donor–acceptor OPVs.^{12,13}

In this work, we investigate the morphological stability of the C_{60} :CuPc interface. We find that ultrathin C_{60} films on top of CuPc are unstable under even relatively low-temperature annealing conditions, resulting in large-scale lateral dewetting. This interpretation is unambiguously revealed by a combination of AFM imaging and NEXAFS spectroscopy on the same samples, which distinguishes lateral dewetting from previously asserted vertical phase segregation of CuPc.¹⁴ Direct AFM observation of the dewetting process suggests a surface

Received: July 8, 2013

Revised: November 19, 2013

Published: November 20, 2013



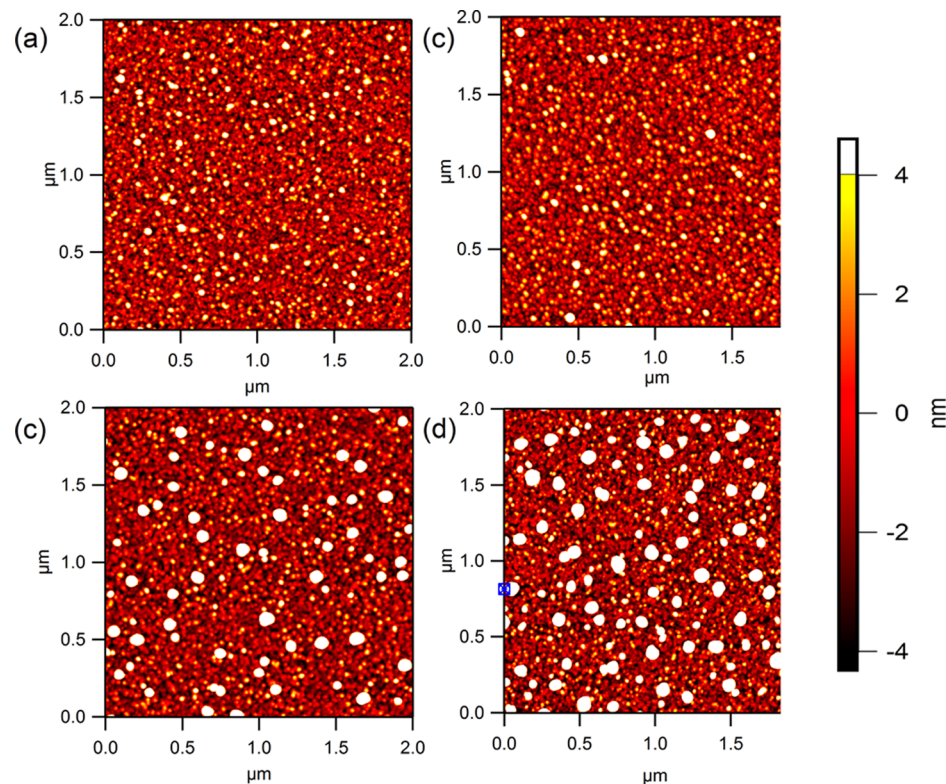


Figure 1. $2 \mu\text{m} \times 2 \mu\text{m}$ AFM images collected in noncontact mode of nominal $1.9 \pm 0.3 \text{ nm } \text{C}_{60}/10 \pm 1 \text{ nm CuPc/silicon}(100)$: (a) as-grown and annealed at 105°C for times of (b) 30 min, (c) 5 h, and (d) 48 h.

diffusion-mediated ripening of C_{60} clusters at the interface that implies significant surface diffusivity and a strong tendency for phase segregation that needs to be considered as part of small-molecule OPV processing strategies. Moreover, the dewetting process could be implemented as a means to controllably nanostructure donor–acceptor interfaces in order to achieve a comblike morphology that would simultaneously optimize carrier transport and exciton dissociation allowing for thicker OPV devices with increased light absorption and J_{sc} .

II. EXPERIMENTAL METHODS

Four bilayer samples of $1.9 \pm 0.3 \text{ nm } \text{C}_{60}/10 \pm 1 \text{ nm CuPc/silicon}(100)$ were prepared in parallel by sequential deposition in a UHV chamber with a base pressure of $< 1 \times 10^{-8}$ Torr. The C_{60} (98%) and CuPc (95%) were obtained from Sigma-Aldrich and loaded, as received, into quartz and boron nitride crucibles, respectively, followed by several hours of outgassing in high vacuum prior to film growth. A silicon(100) wafer with native oxide was cleaved, then sonicated in acetone followed by isopropyl alcohol for 15 min each, and then immediately loaded into the UHV chamber for deposition. The CuPc and C_{60} thin film layers were then grown at $< 6 \times 10^{-7}$ Torr by thermal evaporation from the heated crucibles. A quartz crystal monitor (QCM) was used to monitor the growth rate and thickness of each layer. Samples were thermally annealed at 105°C for 30 min, 5 h, and 48 h in a dry nitrogen glovebox with ~ 2 ppm of oxygen and 1–5 ppm of H_2O . This annealing temperature was chosen for direct comparison with a recent study reporting vertical phase separation in the same system.¹⁴ Moreover, it is within the range of temperatures relevant to small-molecule OPV processing for enhancing charge transport.^{2,15–17} A separate sample prepared in the same way was annealed at a higher temperature of 150°C for comparison. Films of pure

CuPc were prepared using identical procedures, and it was confirmed that no changes in these films were observable after annealing.

Total electron yield near-edge X-ray absorption fine structure (TEY NEXAFS) spectra were collected at Beamline 6.3.2 at the Advanced Light Source.¹⁸ Carbon K-edge spectra were obtained for the photon energy range from 270 to 400 eV. The data were normalized to the incident photon beam intensity measured by a photodiode. Atomic force microscopy was carried out in noncontact mode under ambient conditions using a commercial instrument (Asylum Research MFP-3D). AFM tips (Budget Sensors, Tap300AL-G) had a nominal radius of ~ 10 nm and a nominal resonant frequency of ~ 300 kHz. The TEY NEXAFS technique is surface sensitive, and so our use of very thin films of C_{60} allows direct access to interfacial composition changes that would not be possible for thicker films typically used in bilayer OPV's.

III. RESULTS AND DISCUSSION

III.A. AFM Measurements of Film Morphology. The AFM measurements shown in Figure 1 illustrate significant changes in morphology near the bilayer surface due to annealing. Films of C_{60} grown on top of CuPc exhibit a granular morphology as shown in Figure 1a suggestive of small C_{60} aggregates decorating the somewhat larger grains of the CuPc film. This is very similar to the granular growth of C_{60} on top of pentacene films.¹⁹ While no change in film morphology is obvious after 30 min of annealing, after 5 h it is clear that average cluster size has increased in both height and width on the surface (see quantification in section III.C). This growth in cluster size persists for further annealing up to 48 h. In between the large clusters the C_{60} concentration on the surface is reduced, revealing a film morphology consistent with that of a

pure CuPc film grown on SiO_2 annealed at low temperature (less than 150 °C), well-known from our own work and several other studies.²⁰

The morphological changes increase in rate when annealing at higher temperatures as shown in the sequence in Figure 2.

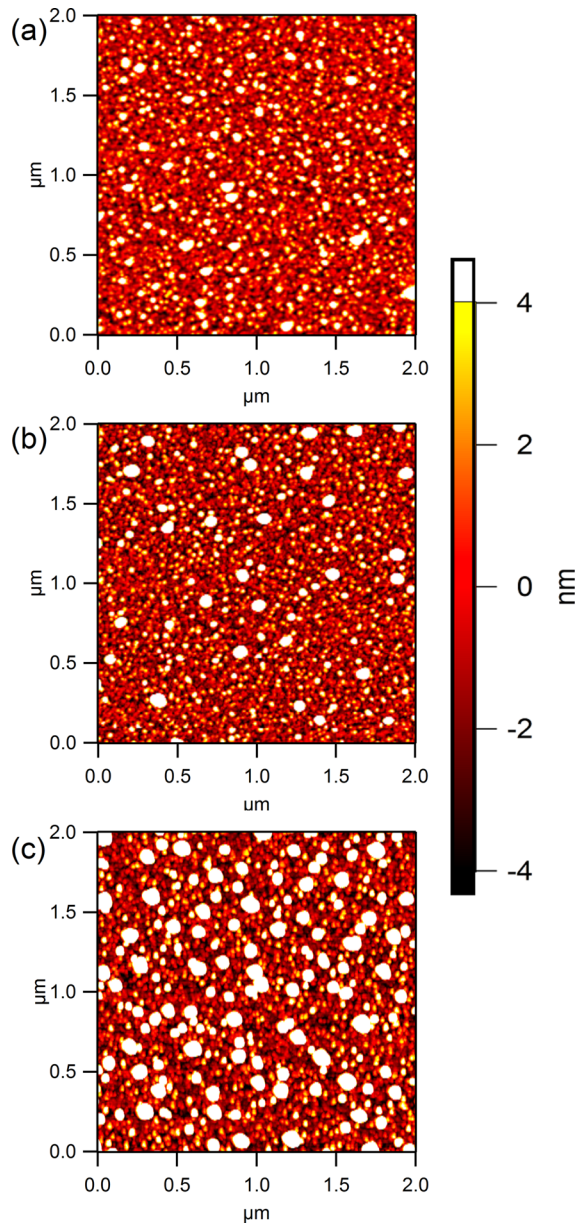


Figure 2. $2 \mu\text{m} \times 2 \mu\text{m}$ AFM images of a $2.2 \pm 0.3 \text{ nm } \text{C}_{60}/10 \pm 1 \text{ nm CuPc}/\text{silicon}(100)$: (a) as-grown; (b) annealed at 100 °C for 30 min; (c) annealed at 150 °C for 30 min.

Here, a somewhat thicker film is imaged so that an increase in surface mound size is more apparent than in Figure 1 after only 30 min of annealing at 100 °C as shown in Figure 2b. Significant mound coarsening is observed after 30 min of annealing a separate film of $2.2 \pm 0.3 \text{ nm } \text{C}_{60}/10 \pm 1 \text{ nm CuPc}/\text{silicon}(100)$ at a higher temperature of 150 °C as shown in Figure 2c. This indicates the expected acceleration of activated surface mass transport as temperature increases.

III.B. NEXAFS Measurements of Film Surface Composition. In order to clarify the composition of the observed 3D mounds on this surface, we carried out TEY NEXAFS on the

same films shown in Figure 1. Figure 3 shows the NEXAFS spectra for the four bilayer films after different annealing

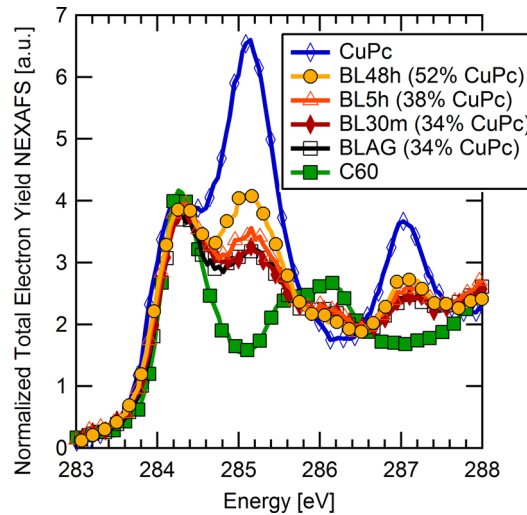


Figure 3. TEY NEXAFS spectra of the carbon K-edge in the region of highest contrast between CuPc and C_{60} . The results of component fitting are shown in the legend in percentage of CuPc.

protocols along with reference spectra for pure C_{60} and CuPc. The NEXAFS spectra for the pure materials show a very convenient anticorrelation just above 285 eV where C_{60} has a local minimum and CuPc has a strong peak due to multiple transitions into its lowest unoccupied molecular orbital.²¹ As a function of annealing time, an enhancement of the CuPc peak is seen in this local region starting with the 5 h annealing time. The relative changes in these spectra can be quantified by fitting the bilayer spectra to linear combinations of the pure material spectra (including also linear and constant background terms). The results of this fitting show that the relative contribution of the pure CuPc to the spectra increase from 34% for the as-grown and 30 min annealed bilayers to 38% after 5 h annealing and 52% after 48 h annealing.

The combination of AFM and NEXAFS leads to the clear conclusion that C_{60} laterally dewets CuPc with annealing. The increase in the exposed surface area of CuPc explains the increase in its relative contribution to the surface-sensitive NEXAFS spectra. The AFM results provide direct morphological evidence that this interpretation is correct via the appearance and thermal coarsening of large C_{60} mounds. Quantitative calculations predicting the NEXAFS composition of the annealed films from mass balance considerations of the AFM data correlate well with the measured values and are shown in the Supporting Information. This conclusion favors an alternate interpretation of recent photoemission studies of similar bilayers of 2 nm C_{60} on CuPc that was interpreted in terms of vertical phase segregation of CuPc toward the surface.¹⁴ Instead of vertical surface segregation, the same results (see Figure 3 of ref 14) could be interpreted as the result of the purely lateral dewetting process visualized in Figures 1 and 2.

III.C. Discussion of C_{60} Dewetting. In order to quantify the dewetting process, we measured the full width at half-maximum and height of a large population of C_{60} mounds observed by AFM under each annealing condition. The results are shown as a plot of mound height as a function of mound width in Figure 4a. The strong correlation between the two

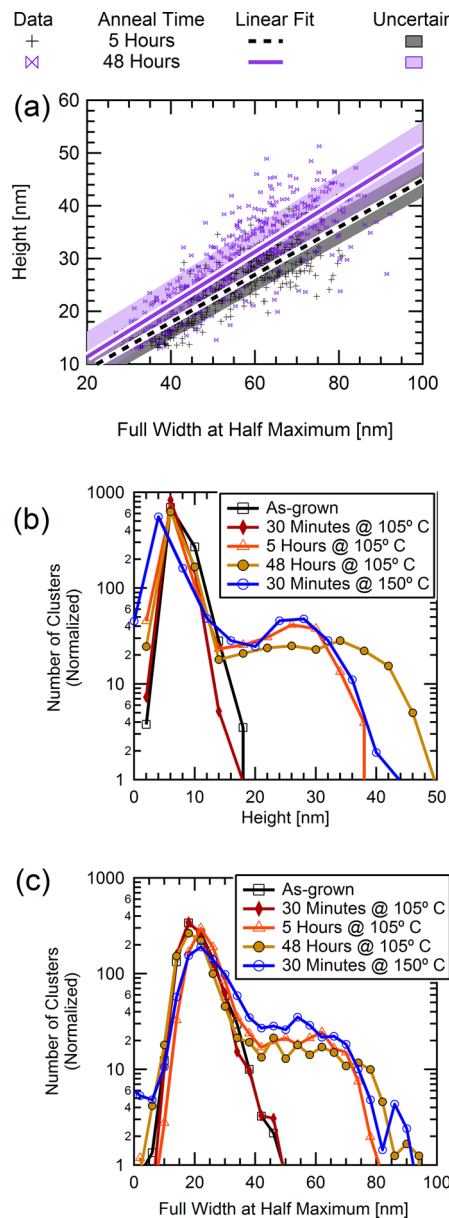


Figure 4. (a) C_{60} cluster height vs fwhm for 5 and 48 h annealing with least-squares linear fit. (b) Normalized histogram of cluster heights for time-dependent annealing at $105\text{ }^{\circ}\text{C}$ and 30 min annealing at $150\text{ }^{\circ}\text{C}$. (c) Normalized histogram of cluster fwhm for same conditions as in part b.

shows that the mounds grow in three dimensions (as opposed to only laterally). Most importantly, the approximate slope of the linear trend for the 5 and 48 h annealing times is nearly identical. This leads to the conclusion that the shape of the mounds is largely determined by near-equilibrium interfacial energetics of the $\text{N}_2:\text{C}_{60}:\text{CuPc}$ system. The size of the mounds may then be inferred to grow primarily as a result of kinetic processes as opposed to a thermally induced mound reshaping.

The observation of dewetting coupled with the known surface energies, $35.1 \times 10^{-3}\text{ J m}^{-2}$ for CuPc²² and $48.1 \times 10^{-3}\text{ J m}^{-2}$ for C_{60} ,²³ leads to the conclusion that the dewetted mounds are composed of nearly pure C_{60} . If the film morphology was driven by vertical phase separation of CuPc to the surface and C_{60} to the substrate, the surface would evolve toward the morphology of pure CuPc films in which dewetting

is unfavorable to minimize the surface energy due to increased surface area. Similarly, if the CuPc and C_{60} tended toward a homogeneously mixed film, the increased surface area from dewetting would also be unfavorable. The presence of dewetting necessitates that the two materials do not have significant intermixing. The higher surface energy of C_{60} favors large 3D mounds of C_{60} over smaller clusters to minimize its surface energy with an increased ratio of volume to surface area. Even though C_{60} mound coarsening increases the surface area of exposed CuPc, this is compensated by the lower surface energy of CuPc and minimizes the free energy of the system.

In Figures 4b and 4c we plot a normalized histogram of mound heights and widths, respectively, that illustrate significant changes due to the thermally induced dewetting process. The as-grown and 30 min-annealed samples are once again almost identical and have a single peak histogram with a roughly Gaussian distribution of heights centered just below 10 nm. Further annealing results in the emergence of a second peak in the height and width histograms that is not present in the as-grown films or films annealed for 30 min. This new second peak corresponds to the population of dewetted C_{60} mounds. The total number of smaller mounds and the average height of these mounds both decrease with annealing time, while the larger mounds continue to grow. This is consistent with surface diffusion-limited mound ripening as described for alloys and thin films.^{24,25} We also note that the C_{60} surface diffusion implied by the dewetting rate is comparable to the reported dewetting of a planar organic on SiO_2 .²⁶ In general, the surface diffusion coefficients at organic–organic interfaces have been predicted²⁷ to be sizable, allowing large-scale surface rearrangements with only modest annealing. Finally, at $150\text{ }^{\circ}\text{C}$ after only about 30 min, the degree of C_{60} island coarsening is intermediate between the images shown in Figure 1c,d, consistent with a thermally activated surface diffusion process. The mound height and width distributions for this annealing protocol are shown in Figure 4b,c.

The observation of C_{60} dewetting at a CuPc interface illustrates two important facts about the $\text{C}_{60}:\text{CuPc}$ interface: (1) surface diffusion of C_{60} on CuPc is significant even at mild annealing temperatures, and (2) interfacial energies between these two materials are generally unfavorable. The latter point suggests a strong tendency for phase segregation that is known for polymer–fullerene heterojunctions and has also been indicated by AFM observations of mixed, codeposited $\text{C}_{60}:\text{CuPc}$ films deposited on heated substrates.¹⁰ Recent work has also shown that solvent-vapor annealing results in a roughening of the fullerene surface in a combined solution-vacuum-deposited solar cell.²⁸ This roughening is explained by the annealing induced lateral dewetting process we describe here. While such uncontrolled processes may be a disadvantage to device performance, they could also be exploited as a mechanism for nanoscale interfacial morphology control. By tuning annealing time (or temperature) during sequential thin layer deposition, it is possible that nanoscale morphologies could be created that would simultaneously optimize exciton dissociation and carrier mobility.²⁹

Enhancements in device performance have been made by adding a mixed³⁰ and graded³¹ layer in between the CuPc and C_{60} layers. The increased donor–acceptor interface area increases the J_{sc} but reduces the fill factor due to recombination at these interfaces as well as decreased carrier mobility. A fully intermixed assembly of $\text{C}_{60}:\text{CuPc}$ for example, would lead to strong recombination effects that degrade device perform-

ance.³² Incorporation of dewetting and/or phase-separation-controlled structures into the production and processing of OPV devices may lead to improved device performance and stability in this system. This is analogous to extensive considerations of annealing³³ and solvent-vapor annealing³⁴ that have been used for morphology-driven efficiency improvement in solution-phase BHJ growth. One possible strategy would be to use dewetting of C₆₀ as a mechanism to create columnar fullerene structures that have recently been reported to allow improvements in BHJ solar cell performance.¹² Further characterization of these kinds of film processing strategies for small molecule films will ideally lead to control of domain sizes in the active layer that is crucial for efficient exciton dissociation and also for control of crystallinity, which is connected to carrier mobility.

IV. SUMMARY AND CONCLUSIONS

In conclusion, we have combined AFM and NEXAFS to demonstrate dewetting at the technologically relevant C₆₀:CuPc interface. By considering very thin 2 nm C₆₀ films grown on CuPc, we could combine surface sensitive spectroscopy and real-space imaging to reveal lateral dewetting due to annealing at 105 °C. This process is to be distinguished from the vertical CuPc segregation proposed to occur for similar C₆₀:CuPc bilayers.¹⁴ Our combined microscopy and spectroscopy results show that CuPc does not transport vertically to the surface for bilayers with C₆₀. They contribute compelling evidence for the strong tendency toward phase segregation in the C₆₀:CuPc system, even in bulk codeposited films,¹⁰ that needs to be incorporated into new strategies for small molecule solar cell morphology optimization. In particular, the implications of these observations extend beyond vacuum-deposited bilayer photovoltaics to situations where C₆₀ interfaces with solution-grown layers are subjected to solvent-vapor annealing that roughens the C₆₀ surface.²⁸ Alternately, a strategy to engineer morphology could use multilayered C₆₀:CuPc with individual layers only ~5–10 nm thick, for which controlled annealing could yield a complex heterostructure with domains the size of the exciton diffusion length. This would improve the fill factor of these devices and allow for a thicker active layer with a higher J_{sc} , leading to much higher PCE. It is plausible that the lateral dewetting behavior of C₆₀ on CuPc is not unique and may occur for C₆₀ bilayers with other donor materials. Finally, it is reasonable also to extrapolate this observation even to the case of mixed fullerene films, whose morphology is likely to be strongly influenced by phase segregation.

ASSOCIATED CONTENT

Supporting Information

Details of quantitative analysis of NEXAFS spectra. This material is available free of charge via the Internet at <http://pubs.acs.org>.

AUTHOR INFORMATION

Corresponding Author

*E-mail dbdouge@ncsu.edu, Ph 919-513-2610.

Notes

The authors declare no competing financial interest.

ACKNOWLEDGMENTS

This work was equally supported by the U.S. Department of Energy (DE-FG02-98ER45737) and NSF CAREER Award

DMR-1056861. T.M. and E.H.G. were at times also supported by GAANN Fellowships.

REFERENCES

- (1) Peumans, P.; Forrest, S. R. Very-High-Efficiency Double-Heterostructure Copper Phthalocyanine/C-60 Photovoltaic Cells. *Appl. Phys. Lett.* **2001**, *79*, 126–128.
- (2) Riede, M.; Mueller, T.; Tress, W.; Schueppel, R.; Leo, K. Small-Molecule Solar Cells - Status and Perspectives. *Nanotechnology* **2008**, *19*, 424001.
- (3) Deibel, C.; Dyakonov, V. Polymer-Fullerene Bulk Heterojunction Solar Cells. *Rep. Prog. Phys.* **2010**, *73*, 096401.
- (4) Xue, J. G.; Uchida, S.; Rand, B. P.; Forrest, S. R. Asymmetric Tandem Organic Photovoltaic Cells with Hybrid Planar-Mixed Molecular Heterojunctions. *Appl. Phys. Lett.* **2004**, *85*, 5757–5759.
- (5) Verlaak, S.; Beljonne, D.; Cheyns, D.; Rolin, C.; Linares, M.; Castet, F.; Cornil, J.; Heremans, P. Electronic Structure and Geminate Pair Energetics at Organic–Organic Interfaces: The Case of Pentacene/C60 Heterojunctions. *Adv. Funct. Mater.* **2009**, *19*, 3809–3814.
- (6) Rand, B. P.; Cheyns, D.; Vasseur, K.; Giebink, N. C.; Mothy, S.; Yi, Y.; Coropceanu, V.; Beljonne, D.; Cornil, J.; Brédas, J.-L.; et al. The Impact of Molecular Orientation on the Photovoltaic Properties of a Phthalocyanine/Fullerene Heterojunction. *Adv. Funct. Mater.* **2012**, *22*, 2987–2995.
- (7) Chen, Y.-H.; Lin, L.-Y.; Lu, C.-W.; Lin, F.; Huang, Z.-Y.; Lin, H.-W.; Wang, P.-H.; Liu, Y.-H.; Wong, K.-T.; Wen, J.; et al. Vacuum-Deposited Small-Molecule Organic Solar Cells with High Power Conversion Efficiencies by Judicious Molecular Design and Device Optimization. *J. Am. Chem. Soc.* **2012**, *134*, 13616.
- (8) Pandey, R.; Holmes, R. J. Graded Donor-Acceptor Heterojunctions for Efficient Organic Photovoltaic Cells. *Adv. Mater.* **2010**, *22*, 5301–5305.
- (9) Peumans, P.; Uchida, S.; Forrest, S. R. Efficient Bulk Heterojunction Photovoltaic Cells Using Small-Molecular-Weight Organic Thin Films. *Nature* **2003**, *425*, 158–162.
- (10) Opitz, A.; Wagner, J.; Brutting, W.; Hinderhofer, A.; Schreiber, F. Molecular Semiconductor Blends: Microstructure, Charge Carrier Transport, and Application in Photovoltaic Cells. *Phys. Status Solidi A* **2009**, *206*, 2683–2694.
- (11) Chen, G.; Sasabe, H.; Wang, Z. Q.; Wang, X. F.; Hong, Z. R.; Yang, Y.; Kido, J. J. Co-Evaporated Bulk Heterojunction Solar Cells with >6.0% Efficiency. *Adv. Mater.* **2012**, *24*, 2768.
- (12) Thomas, M.; Worfolk, B. J.; Rider, D. A.; Taschuk, M. T.; Buriak, J. M.; Brett, M. J. C60 Fullerene Nanocolumns–Polythiophene Heterojunctions for Inverted Organic Photovoltaic Cells. *ACS Appl. Mater. Interfaces* **2011**, *3*, 1887.
- (13) Yang, F.; Forrest, S. R. Photocurrent Generation in Nanostructured Organic Solar Cells. *ACS Nano* **2008**, *2*, 1022.
- (14) Wei, H. X.; Li, J.; Xu, Z. Q.; Cai, Y.; Tang, J. X.; Li, Y. Q. Thermal Annealing-Induced Vertical Phase Separation of Copper Phthalocyanine: Fullerene Bulk Heterojunction in Organic Photovoltaic Cells. *Appl. Phys. Lett.* **2010**, *97*, 083302.
- (15) Fitzner, R.; Mena-Osteritz, E.; Mishra, A.; Schulz, G.; Reinold, E.; Weil, M.; Karner, C.; Ziehlke, H.; Elschner, C.; Leo, K.; et al. Correlation of π -Conjugated Oligomer Structure with Film Morphology and Organic Solar Cell Performance. *J. Am. Chem. Soc.* **2012**, *134*, 11064.
- (16) Schultes, S. M.; Sullivan, P.; Heutz, S.; Sanderson, B. M.; Jones, T. S. The Role of Molecular Architecture and Layer Composition on the Properties and Performance of CuPc-C60 Photovoltaic Devices. *Mater. Sci. Eng., C* **2005**, *25*, 858.
- (17) Suemori, K.; Miyata, T.; Hiramoto, M.; Yokoyama, M. Enhanced Photovoltaic Performance in Fullerene:Phthalocyanine Codeposited Films Deposited on Heated Substrate. *Jpn. J. Appl. Phys.* **2004**, *43*, L1014.
- (18) Underwood, J. H.; Gullikson, E. M. High-Resolution, High-Flux, User Friendly VLS Beamline at the ALS for the 50–1300 eV Energy Region. *J. Electron Spectrosc. Relat. Phenom.* **1998**, *92*, 265.

- (19) Conrad, B. R.; Tosado, J.; Dutton, G.; Dougherty, D. B.; Jin, W.; Bonnen, T.; Schuldenfrei, A.; Cullen, W. G.; Williams, E. D.; Reutt-Robey, J. E.; et al. C-60 Cluster Formation at Interfaces with Pentacene Thin-Film Phases. *Appl. Phys. Lett.* **2009**, *95*, 213302.
- (20) Miller, C. W.; Sharoni, A.; Liu, G.; Colesniuc, C. N.; Fruhberger, B.; Schuller, I. K. Quantitative Structural Analysis of Organic Thin Films: An X-ray Diffraction Study. *Phys. Rev. B* **2005**, *72*, 104113.
- (21) De Francesco, R.; Stener, M.; Fronzoni, G. Theoretical Study of Near-Edge X-ray Absorption Fine Structure Spectra of Metal Phthalocyanines at C and N K-Edges. *J. Phys. Chem. A* **2012**, *116*, 2885.
- (22) Gao, J.; Asadi, K.; Xu, J. B.; An, J. Controlling of the Surface Energy of the Gate Dielectric in Organic Field-Effect Transistors by Polymer Blend. *Appl. Phys. Lett.* **2009**, *94*, 093302.
- (23) Tajima, Y.; Matsuura, T.; Numata, Y.; Yamazaki, D.; Kawamura, H.; Osedo, H. Surface Free Energy and Wettability Determination of Various Fullerene Derivative Films on Amorphous Carbon Wafer. *Jpn. J. Appl. Phys.* **2008**, *47*, 5730–5733.
- (24) Chakraverty, B. K. Grain Size Distribution in Thin Films. I. Conservative Systems. *J. Phys. Chem. Solids* **1967**, *28*, 2401.
- (25) Lifshitz, I. M.; Slyozov, V. V. The Kinetics of Precipitation from Supersaturated Solid Solutions. *J. Phys. Chem. Solids* **1961**, *19*, 35.
- (26) Kowarik, S.; Gerlach, A.; Sellner, S.; Cavalcanti, L.; Schreiber, F. Dewetting of an Organic Semiconductor Thin Film Observed in Real-time. *Adv. Eng. Mater.* **2009**, *11*, 291–294.
- (27) Cantrell, R. A.; Clancy, P. A New Kinetic Monte Carlo Algorithm for Heteroepitactical Growth: Case Study of C-60 Growth on Pentacene. *J. Chem. Theory Comput.* **2012**, *8*, 1048.
- (28) Zimmerman, J. D.; Xiao, X.; Renshaw, C. K.; Wang, S. Y.; Diev, V. V.; Thompson, M. E.; Forrest, S. R. Independent Control of Bulk and Interfacial Morphologies of Small Molecular Weight Organic Heterojunction Solar Cells. *Nano Lett.* **2012**, *12*, 4366.
- (29) Weickert, J.; Dunbar, R. B.; Hesse, H. C.; Wiedemann, W.; Schmidt-Mende, L. Nanostructured Organic and Hybrid Solar Cells. *Adv. Mater.* **2011**, *23*, 1810.
- (30) Xue, J.; Rand, B. P.; Uchida, S.; Forrest, S. R. A Hybrid Planar–Mixed Molecular Heterojunction Photovoltaic Cell. *Adv. Mater.* **2005**, *17*, 66–71.
- (31) Chen, L.; Tang, Y.; Fan, X.; Zhang, C.; Chu, Z.; Wang, D.; Zou, D. Improvement of the Efficiency of CuPc/C60-Based Photovoltaic Cells Using a Multistep Structure. *Org. Electron.* **2009**, *10*, 724–728.
- (32) Hesse, H. C.; Weickert, J.; Al-Hussein, M.; Dossel, L.; Feng, X.; Mullen, K.; Schmidt-Mende, L. Discotic Materials for Organic Solar Cells: Effects of Chemical Structure on Assembly and Performance. *Sol. Energy Mater. Sol. Cells* **2010**, *94*, 560–567.
- (33) Collins, B. A.; Gann, E.; Guignard, L.; He, X.; McNeill, C. R.; Ade, H. Molecular Miscibility of Polymer:Fullerene Blends. *J. Phys. Chem. Lett.* **2010**, *1*, 3160.
- (34) Chen, L.-M.; Hong, Z.; Li, G.; Yang, Y. Recent Progress in Polymer Solar Cells: Manipulation of Polymer:Fullerene Morphology and the Formation of Efficient Inverted Polymer Solar Cells. *Adv. Mater.* **2009**, *21*, 1434.